Progress in Nuclear Magnetic Resonance Spectroscopy xxx (2010) xxx–xxx

Contents lists available at ScienceDirect

Progress in Nuclear Magnetic Resonance Spectroscopy

journal homepage: www.elsevier.com/locate/pnmrs

Lab-on-a-chip detection by magnetic resonance methods

Elad Harel *

The James Franck Institute at the University of Chicago, 929 E. 57th Street, GCIS E028, Chicago, IL 60637, USA

ARTICLE INFO

Article history:
Received 16 January 2007
Accepted 10 May 2010
Available online xxxx

Keywords:
Microfluidics
Imaging
Microcoils
Remote detection
Flow

Contents

1. Introduction

Over the past decade, there has been a growing interest in departing from the traditional model of bench-top chemistry in which compounds are synthesized on a macroscopic scale that involves milliliter- to liter-sized volumes of reagents. The explosion of growth in microfabrication where device features have become exponentially smaller while increasing in sophistication, has inspired a pursuit of scaling down traditional laboratory tools to the micrometer level for limited sample volumes, waste reduction, greater environmental control, and parallelism, while drastically

* Tel.: +1 773 702 6066.
E-mail address: elharel@uchicago.edu

0079-6565/$ - see front matter
doi:10.1016/j.pnmrs.2010.05.002

Please cite this article in press as: E. Harel, Lab-on-a-chip detection by magnetic resonance methods, Prog. Nucl. Magn. Reson. Spectrosc. (2010), doi:10.1016/j.pnmrs.2010.05.002

cutting down on time and expense. Sophisticated so-called lab-on-a-chip (LOC) platforms are now commercially available [1], with devices fabricated for a host of chemical and biochemical applications including microreactors in synthetic chemistry [2], rapid DNA analysis [3], and proteomics [4] to name a few. Researchers have been able to integrate a host of laboratory tools directly onto the LOC device such as mixers, micropumps, heaters, and separators [5].

Improvements and innovations in device fabrication have progressed in parallel with developments in efficient and sensitive detection. Owing to the small sample volumes, highly sensitive detection methods, mainly in the optical regime, have been applied to analyze the fluid flow and hydrodynamics, which play a central role in the kinetics of the reaction or the fluid mechanics of the separations [6]. Optical detection methods, however, suffer from some drawbacks. While fluorophores provide highly sensitive means of fluid tracking, there is the fear that the hydrodynamic properties of the fluid can be altered at these small dimensions [7]. The vast majority of detection methods are based on laser-induced fluorescence (LIF), which lacks chemical specificity except for naturally fluorescent molecules. Absorption based spectroscopy has been demonstrated, but the short optical path length through the microfluidic channel limits sensitivity [8,9]. Most importantly, all optical methods require transparency in the specific region of the electromagnetic spectrum where they operate. Even when it is possible to perform optical spectroscopy this typically comes at the price of performing imaging. Magnetic resonance (MR) offers a detection modality that can circumvent these limitations as it can image and quantify fluid flow [10] as well as provide a powerful means of chemical identification albeit only in sufficient concentrations [11,12]. For most chemical and biological species, this means relatively large volumes or concentrations, orders of magnitude above that available in small LOC devices.

Faced with these challenges, researchers have proceeded to try and push MR to its detection limit by employing a host of novel techniques, which are the subject of this review. MR has the capability to perform imaging, spectroscopy, and flow simultaneously, while being completely noninvasive. Unlike most of the optic-based techniques in use, there is no need for a tracer, nor is there a need for the device to be transparent, opening up the possibility for a whole new host of materials that could be used in microfabrication. Unfortunately, the noninvasive nature of MR is also responsible for its extremely poor sensitivity since both result from a very weak interaction between the external magnetic field and the nuclear spins. Additionally, motion artifacts make performing spectroscopy and imaging exceptionally challenging on LOC devices. Spectroscopy, even on a static sample, is difficult as the chip geometry strongly distorts the magnetic field homogeneity, resulting in kilohertz linewidths.

Despite these challenges, several groups have made significant headway. Two separate but related approaches have made notable progress in tackling the sensitivity problem associated with detection of mass-limited samples directly on the device. The first involves engineering detectors in which the filling factor is optimized by placing the inductor as close to the sample volume as possible. In the case of LOC this implies planar type geometries that are lithographically fabricated directly onto the device. Several variants of this approach have appeared in the literature, some of which are discussed below. The other method involves a technique called remote detection (RD) that separates the detection and encoding parts of a typical MR experiment so as to optimize each individually. RD is especially suited for LOC applications where the footprint of the device is large relative to the volume of spins responsible for the signal.

2. Theoretical background

2.1. Poor sensitivity of mass-limited samples

MR practitioners are well aware of the sensitivity limitations when dealing with small sample volumes or low concentrations. No more is this problematic than in LOC applications where the fluid volume comprises only a tiny fraction of the detection volume when using conventional RF coils that encompass the whole device. For example, the direct sensitivity of a fluid packet inside a 100-μm wide microfluidic channel inside an LOC device with a surface area of 1 cm^2, is less than 10^{-5} of that available to high-resolution NMR. At low concentrations, the signal is typically below the limit-of-detection (LOD), precluding the use of conventional MR methods. Fortunately, the LOD can be significantly increased by the use of novel techniques that are the subject of this review. A discussion of MR on micrometer samples must first begin with an analysis of the sensitivity of inductive detection. A brief analysis of direct detection using solenoid coils is presented, followed by a discussion of some of the advantages and challenges of planar coils that are suitable for LOC applications.

2.2. Sensitivity of direct detection

The vast majority of NMR experiments fall under the category of direct detection in which both excitation and detection of spins occurs using the same RF transmit and receive coil. The signal-to-noise ratio (SNR) of a direct NMR experiment for large solenoids can be derived by considering the induced *emf* and noise generated by the receiver coil. If one assumes a uniformly excited sample, then the SNR is given by [13]

$$\mathrm{SNR} = \frac{\gamma(B_1/i)V_s N\eta^2\omega_0^2}{4\sqrt{2k_B T_s V_{noise}}}, \tag{1}$$

where B_1/i is the magnetic field per unit current generated by the RF coil, V_s is the sample volume, T_s is the sample temperature, and N is the number of spins. The noise due to the resistance of the coil, R_{noise}, and the bandwidth of the receiver, Δf, is given by

$$V_{noise} = \sqrt{4k_B T R_{noise}\Delta f}. \tag{2}$$

The filling factor, η, is an especially important parameter for LOC applications. As a rough approximation it is given by the ratio of the sample volume to twice the coil volume, $\eta = V_s/2V_c$. This simple formula is adequate only when considering solenoid coils where the induced field is equally split between the interior and exterior of the coil. For other coil geometries, the factor of 2 must be replaced by a geometric factor that adequately describes the proportion of the field felt by the sample. Furthermore, the above SNR relation does not take into account the case of nonuniform excitation, which is important for planar coil geometries. Finally, Eq. (1) no longer applies for smaller coil geometries where the skin depth of the conductor is on the order of the diameter.

2.3. Sensitivity of microsolenoid coils

An in-depth look at the sensitivity of microcoils will serve as a backdrop for a discussion of planar structures as well as an analysis of the sensitivity of remote detection which utilize these types of detectors. Consider a loop of wire that generates a magnetic field per unit current $\mathbf{B}_1/i$ interacting with a dipole $\mathbf{m}$. The induced *emf*, ξ, is given by

$$\xi = \left(-\frac{\partial}{\partial t}\right)\left(\frac{\mathbf{B}_1}{i}\cdot\mathbf{m}\right). \tag{3}$$

Please cite this article in press as: E. Harel, Lab-on-a-chip detection by magnetic resonance methods, Prog. Nucl. Magn. Reson. Spectrosc. (2010), doi:10.1016/j.pnmrs.2010.05.002

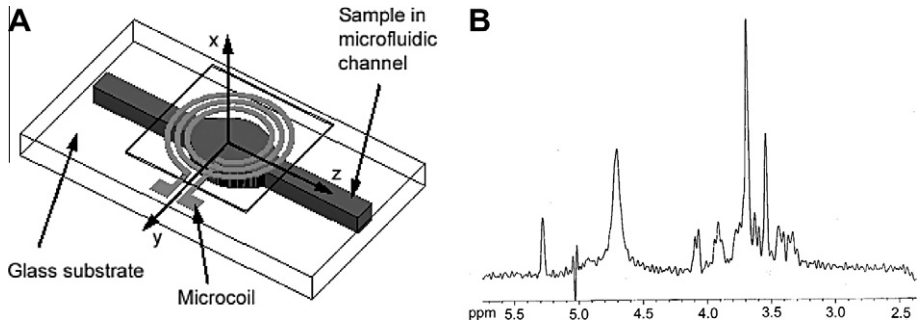

Fig. 1. (A) Three-dimensional schematic of a multi-turn electroplated NMR microcoil. The microfluidic channel is etched below the probe with a sample volume as low as a 30 nL. The coil diameter varies from 500 μm up to about 2 mm. (B) Spectrum at 300 MHz of 160 μg of sucrose in 470 nL of D_2O after Lorentz–Gauss resolution enhancement giving a FWHM of approximately 9 Hz. Reprinted with permission from Massin et al. [16].

The voltage generated by the coil is found by integrating the induced *emf* over the entire sample volume. Immediately following a 90° excitation pulse the signal is given by (ignoring the oscillating part)

$$\xi = \omega_0 M_0 V_s B_1 / i. \tag{4}$$

The signal scales with the square of the magnetic field since the Larmor frequency, ω_0, and magnetization, M_0, scale linearly with the field strength. The noise, however, scales in a more complicated manner per Eq. (2). If one now considers an n-turn solenoid coil with a diameter, $2r$, with turns spaced by $3r$, composed of a conductor with diameter $2a$, permeability μ, and resistivity ρ, the resistance in the coil, R, is given by [14]

$$R = \frac{an}{r}\sqrt{\frac{\mu\mu_0\omega_0\rho}{2}}. \tag{5}$$

The field per unit current is given by

$$\frac{B_1}{i} = \frac{\mu_0 nW}{2r}\left(\left(\frac{a}{r}\right)^2 + (3(n-1)/2)^2\right)^{-1/2}, \tag{6}$$

where W is the power supplied by the RF amplifier. The SNR, therefore, is inversely proportional to the coil radius when the ratio of the inductor diameter to coil diameter, a/r, is kept constant. Smaller coils, in principle, produce the highest possible sensitivity. In practice, however, this scaling is not as favorable because the uniformity of the current flow in the conductor decreases with coil dimensions. Application of an alternating current to the coil induces eddy currents that oppose the main current in the center of the wire, while enhancing the current near the outer perimeter in a region given by the skin depth

$$\lambda = \frac{1}{\sqrt{\mu\pi\sigma f}}, \tag{7}$$

where σ and f are the conductivity of the wire and frequency of the applied current, respectively. Introducing the dimensionless unit, $z = 2a/\lambda$, one can define two regimes: the skin-depth regime where the diameter of the wire is much larger than the skin-depth ($z \geqslant 8$) and the uniform-current regime where the skin-depth is on the order of the diameter ($z \leqslant 2$). The SNR per unit volume scales differently with the coil diameter in each regime

$$\mathrm{SNR}_{puv} \alpha \frac{\omega_0^{7/4}}{2r}, \quad z \geqslant 8; \tag{8}$$

$$\mathrm{SNR}_{puv} \alpha \frac{\omega_0^2}{\sqrt{2r}}, \quad z \leqslant 2. \tag{9}$$

While decreasing the size of the coil increases the sensitivity per unit volume, it approaches a region of diminishing returns. Winding a fine copper wire around a small glass capillary [15] provides excellent field homogeneity and high sensitivity, but coil fabrication becomes impractical at diameters less than about 200 μm.

3. Direct lab-on-a-chip detection

3.1. Planar detectors

For LOC applications, microcoils are, in general, not applicable because of their non-planar geometry. NMR coils built using photolithographic techniques [16,17] are capable of direct integration into LOC devices. These planar microstructures can be batch-fabricated with features as small as 1 μm. The major challenge of successful integration of such devices is in achieving high magnetic field homogeneity and sensitivity, comparable to that achievable by microsolenoid coils.

As with solenoid coils, the signal depends on the magnetic field per unit current generated by the RF coil. For planar geometries, this field is highly inhomogeneous in magnitude and direction so that B_1 in Eq. (1) must be replaced with $\mathbf{B}_1(\mathbf{r})$ instead. In general, this problem becomes too difficult to solve analytically for realistic coil geometries, and one must resort to numerical finite-element modeling (FEM). Massin et al. [16], have calculated and experimentally measured the sensitivity of a planar microcoil with N turns and inner diameter, D_i, schematically shown in Fig. 1A. The microfluidic channel directly below the coil was fabricated by first etching one side of two Pyrex-glass wafers using HCl through a patterned poly-silicon mask before fusing them together at high temperature (~600 °C). The NMR coils themselves are fabricated by SU-8 photoepoxy and copper electroplating as described in detail elsewhere [18]. An experimental spectrum of 1 M-sucrose solution in D_2O is shown in Fig. 1B.

The effects of the coil itself on the magnetic field inhomogeneity can be appreciated by considering the distortions created when plunging a coil of a cylindrical geometry into a perfectly homogeneous static field. The calculated linewidth for a coil with a diameter to height ratio of about 3 is nearly 30 Hz, and improves with larger diameter to height ratios. Nonetheless, this figure is representative of the challenges of using planar microcoils with susceptibility mismatch between the conductor and sample at such close proximity. Moving the coil further from the sample improves homogeneity at the cost of lower SNR as the field strength experienced by the sample decreases. Since magnetic field inhomogeneity affects both the lineshape and the SNR, this is the single most important factor that must be improved for planar microcoils to be viable in high-resolution NMR.

A promising alternative to planar microcoils are stripline detectors, which are simple to fabricate and achieve superb sensitivity and spectral resolution [19]. A stripline is a two-dimensional analog of a wire positioned parallel to the static magnetic field as

Please cite this article in press as: E. Harel, Lab-on-a-chip detection by magnetic resonance methods, Prog. Nucl. Magn. Reson. Spectrosc. (2010), doi:10.1016/j.pnmrs.2010.05.002

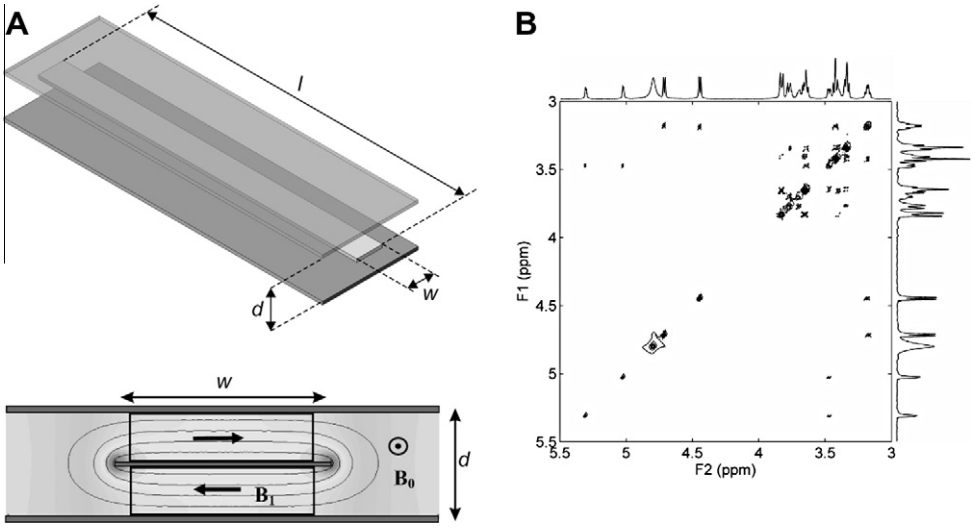

Fig. 2. (A) Top – 3D schematic of stripline NMR probe employing a self-resonant design. The central strip is designed with a $\lambda/2$ length and contains a constriction to concentrate the local current density in the vicinity of the sample. The ground planes above and below the central strip allow for improved homogeneity. Bottom – Cross-sectional field pattern showing the RF homogeneity perpendicular to the static field direction. (B) 600 MHz ^{1}H–^{1}H COSY spectrum of 1.2 μmol ^{13}C-labeled glucose after 13.6 h of total acquisition time. Reprinted with permission from Bart et al. [19].

shown in Fig. 2A. A current passed through an infinite wire in this orientation will generate a field perpendicular to the static field with no disruption to the field homogeneity. Since the B_1 field drops off with the inverse of the distance from the wire, it is necessary sandwich the wire or strip between two parallel ground planes to provide improved homogeneity. Instead of using a lossy LC circuit, the stripline can be designed as a self-resonating structure if its length matches an integer number of half wavelengths at the Larmor frequency. To maximize the field generated by such a standing wave inside the resonant cavity, a constriction can be implemented that increases the current density in the region of the sample. The RF homogeneity of the stripline detector, measured as the ratio of the signal amplitude following an 810° pulse to that of a 90° pulse, was found to be 76% (higher values could be obtained by using susceptibility matching plugs). The LOD was found to be around 3×10^{14} spins/$\sqrt{}$Hz, and the spectral resolution after careful shimming was less than 1 Hz. The spectral resolution and RF homogeneity in the stripline detector are on a par with commercial probes available for use with high-resolution NMR as demonstrated by the two-dimensional ^{1}H–^{1}H COSY spectrum of glucose in D_2O shown in Fig. 2B. The sensitivity has the potential for further optimization by eliminating electrical losses caused by the silicon substrate.

Conceptually similar to the stripline, detection of nuclear spins by a planar microslot waveguide was recently demonstrated by Maquire et al. [20]. These structures are used to transport quasi-transverse electromagnetic mode (TEM) RF signals on dielectric materials. Impressively, the waveguide was able to obtain a two-dimensional spectrum of ribonuclease-A on approximately 10^{14} spins. Although the device has not yet been implemented directly into an LOC device, the favorable scaling of the sensitivity with reduced size, planar geometry, and high sensitivity make future integration possible.

3.2. Direct imaging

With only a few exceptions, direct detection of MR on LOC devices has dealt exclusively with spectroscopy of localized regions of the device. Microcoils, planar ones in particular, have a few serious drawbacks that make them a poor choice for imaging applications. First, the relatively large fingerprint of planar microcoils, on the order of 1–2 mm in diameter, means that there are only a few structures that can be practically fabricated on a single device [21]. The structures themselves are orders of magnitude larger than the desired spatial resolution, and while imaging gradients could in principle be used in conjunction with microcoils, the sensitivity loss would to a large degree negate the advantages of using a smaller detector in the first place. For striplines or microslot waveguides, the high spectral resolution in large part depends on the structure being much larger than the sample so at to eliminate magnetic field distortions near the detection region. Even if one could significantly reduce the size of the detectors, mutual coupling between neighbors would preclude their use. The packing density would then be significantly less than the spatial resolution. Finally, from a practical standpoint the integration of parallel detectors would increase the complexity of the electronics since each detector would require its own transmitter and receiver channel, making this approach expensive and impractical.

The few published works on imaging LOC devices have utilized large-area planar surface coils to measure the motion distributions of the flowing fluids using standard velocity encoding pulse sequences. While the filling factor for such coils is relatively poor, these detectors are suitable for fluid flow measurements when the analyte is at a very high concentration or pure as in the case of water. NMR microscopy [10] allows not only the spin density or relaxation to be imaged, but also allows encoding of the velocity, acceleration, and diffusion by exploiting the reversible nature of pulsed magnetic fields interacting with the nuclear spins. The phase, $\phi(T)$, accumulated by spins with a time-dependent position vector described by $\mathbf{r}(t)$ due solely to a pulsed gradient (or series of gradients), $\mathbf{G}(t)$, over a period of time, T, is given by

$$\phi(T) = \gamma \int_0^T \mathbf{G}(t) \cdot \mathbf{r}(t)\, dt. \tag{10}$$

For a flowing sample, the position can be expanded in a Taylor series to give

$$\phi(T) = \gamma \int_0^T \mathbf{G}(t) \cdot \mathbf{r}(0)\, dt + \gamma \int_0^T \mathbf{G}(t) \cdot \mathbf{v}(0) t\, dt + O(t^2). \tag{11}$$

The first term in the expansion gives phase accumulation due to the initial position of the spins, while the first-order term adds an additional phase factor proportional to the initial velocity $\mathbf{v}(0)$. The

Please cite this article in press as: E. Harel, Lab-on-a-chip detection by magnetic resonance methods, Prog. Nucl. Magn. Reson. Spectrosc. (2010), doi:10.1016/j.pnmrs.2010.05.002

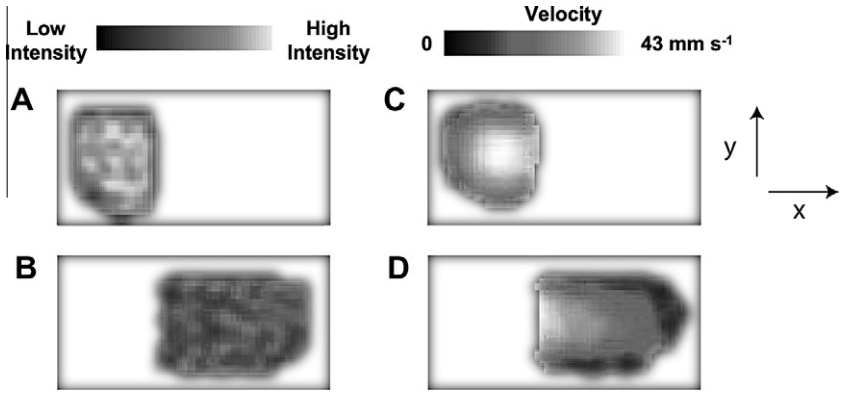

Fig. 3. Cross-sectional images of immiscible flow through a microfluidic channel of two fluids converging. Spin density and velocity maps of oil (A and C) and water (B and D), respectively. Reprinted with permission from [23].

acceleration and higher-order terms are often neglected for laminar flows that dominate in most LOC devices discussed here. To isolate only the initial spin density, the velocity contribution can be nulled by adjusting the pulsed gradients such that $\int_0^T \mathbf{G}(t)t\,dt = 0$ while $\int_0^T \mathbf{G}(t)\,dt \neq 0$. Similarly, the velocity can be encoded by reversing this set of conditions.

Using gradient encoding methods, Ahola et al. [22] measured the velocity distribution of water flowing through a commercial micromixer at a spatial resolution of 29 μm × 43 μm using an external surface coil matched to the area of the LOC device. In another example, Akpa et al. [23] used a conventional birdcage coil to measure the mixing of two immiscible fluids inside a simple LOC T-mixer. Cross-sectional images of the spin density as well as the velocity distribution through a channel where the fluids converge are shown in Fig. 3.

4. Remote detection

4.1. Introduction to remote detection

Integrating planar detectors into the chip directly is less attractive for LOC applications than optical methods since it significantly alters more established chip fabrication protocols. While specialized devices may be fabricated for use with MR detection methods, the vast majority of devices to come out of the greater LOC community are generally excluded. The assumption underlying the need for direct coil integration that can achieve high sensitivity and spectral resolution is that encoding and detection of the nuclear spins occurs in the same physical location in space in line with conventional high-resolution NMR. However, this restriction can be eliminated if the sample is transported from one location to another, as is the case with LOC devices. In the next section, a method called remote detection is described which offers some flexibility in the integration of unmodified LOC devices under certain conditions.

4.2. Basic principles of remote detection

Remote detection (RD) is a general method for increasing the sensitivity in an MR experiment, which is applicable when excitation and detection can be separated in some manner [24]. In its most common implementation, RD involves actual physical separation of encoding and readout such that information about a species in one environment is detected by examination of it in another. Typically, a large RF coil that encompasses the sample performs the encoding step while a smaller coil concentrates the signal for more efficient and sensitive detection. In fact, such a separation allows for the possibility of moving away from inductive detection altogether and implementing non-inductive schemes such as optical detection [25].

Regardless of the detection modality, the principle remains the same. Fig. 4 illustrates a generic RD scheme. At equilibrium, the nuclear spins are aligned along the static field. A selective pulse excites a subset of spins spatially or spectrally (spatiospectral selection is also possible). As with any other MR pulse sequence, the excited spins acquire phase due to a combination of free evolution and a well-defined sequence of RF and gradient pulses that place the magnetization into a desired spin state (Fig. 4A). In conventional MR experiments, readout is performed at this junction. In contrast, for RD, the phase of the spins in the transverse plane is stored along the longitudinal direction where the spin state is preserved for the duration of the spin–lattice relaxation, T_1. The spins then rapidly flow out to the detector before an irreversible loss in signal occurs. At the detection stage, a train of pulses provides information about the phase of the stored magnetization. RD can be considered a two-dimensional experiment where the direct dimension is physically separated from the indirect dimension.

For sensitivity purposes, the detector is arranged to have a smaller volume than the encoding volume in most cases, and several pulses are needed to completely detect the encoded magnetization. The set of points of integrated signal intensity from the pulse train comprises a travel curve that measures the time-of-flight (TOF) between encoding and detection (Fig. 4B). The spins that are first to arrive are typically unencoded leading to a maximum in the signal. As encoded spins arrive they mix with unencoded spins causing a decrease in the overall signal as observed by a dip in the TOF curve. The steady-state signal is restored once the encoded spins leave the detector.

The most significant difference between direct and remote detection is that in the latter the readout dimension is no longer available since the encoding coil is used only to manipulate the magnetization rather than detect it. As a consequence, encoding must proceed point-by-point. For example, a free-induction decay (FID) is typically measured by exciting the spins into the transverse plane and recording the subsequent transient signal. In RD, points along the FID are recorded by delaying the time between the storage and detection pulses, such that each point in the travel curve contributes exactly one point to the indirect interferrogram (e.g. FID, Fig. 4C) built up by repeating the remote experiment, each time with a different indirect point (i.e. time delay).

4.3. Remote detection pulse sequence

In principle any pulse sequence can be used in RD as long as the desired phase information about the signal can be transferred onto

Please cite this article in press as: E. Harel, Lab-on-a-chip detection by magnetic resonance methods, Prog. Nucl. Magn. Reson. Spectrosc. (2010), doi:10.1016/j.pnmrs.2010.05.002

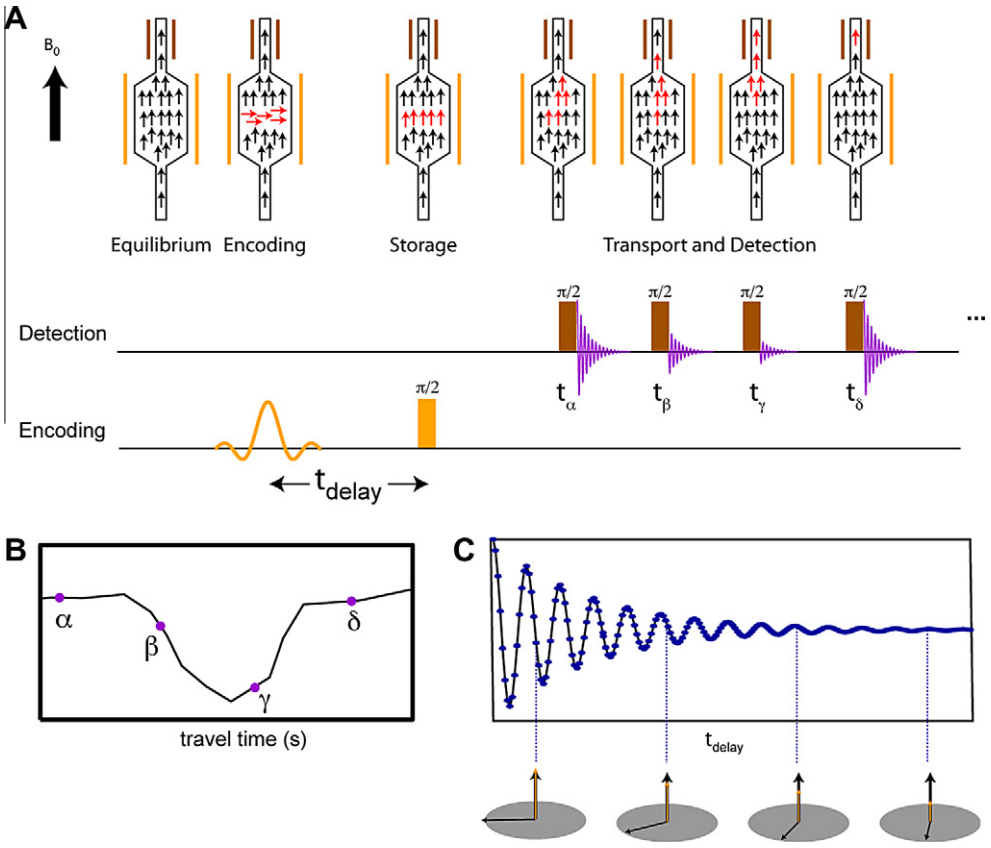

Fig. 4. (A) General remote detection scheme. A selective pulse excites the spins of interest. The magnetization precesses about the static field, acquiring phase which gives either spectroscopic (free evolution) or imaging (evolution in the presence of gradients) information about the sample. A $\pi/2$ storage pulse converts the phase information into longitudinal magnetization, which is subject only to T_1 relaxation during travel to the detector. The spins then flow to the detector, which reads out the amplitudes by a train of hard $\pi/2$ pulses. (B) Each detection pulse contributes one point to the time-of-flight (TOF) curve. (C) Repeating the experiment point-by-point creates an interferogram that decays, i.e. the free-induction decay (FID). In the case of spectroscopy, this corresponds to incrementing the delay between the encoding and storage pulses. In the case of imaging, the delay is fixed and the gradient strength is incremented so as to sample *k*-space (the reciprocal space in which the signal is acquired prior to Fourier transformation). Each detection pulse then creates a partial image corresponding to the spin density in the sample, which arrives at the same TOF to the detector. The sum of these partial images creates the full image of the sample.

the spin sensor. Instead of readout at the end of a particular pulse sequence, a hard, 90° pulse stores one component of the phase of the signal in the transverse plane onto the longitudinal axis. To reconstruct the complex data signal, a two-step phase cycle in which the storage pulse is phase shifted by 90° is necessary. The signal measured at the detector is proportional to the longitudinal magnetization times a factor that depends on the detection volume, fraction of encoded spins, and relaxation rate of the spin sensor. Since the detection volume may not be matched to the encoded volume, and in most cases is much smaller, it is crucial that the spacing between detection pulses is chosen such that no encoded spins go undetected. It is also important to take into account the fraction of unencoded spins in the detector since these add an unwanted baseline to the signal that shows up in the center of the image or spectrum. For flow that is stable over the course of the entire acquisition, the baseline is constant for each indirect point in the experiment, and can be removed after a single measurement. More commonly, the baseline can exhibit slow drifts and two additional phase cycling steps that invert the phase of the storage pulse are needed. In all, the weighted signal after a four-step phase cycle $(x,-x,y,-y)$ of the storage pulse, is proportional to

$$S(t_1) \propto 2\xi\lambda M(t_1)e^{i\theta}, \tag{12}$$

where ξ is the fraction of encoded signal in the detector, λ is factor related to the longitudinal relaxation of the spins, θ is the desired phase, and $M(t_1)$ is the amplitude of the transverse magnetization.

4.4. Sensitivity of remote detection

The original motivation behind RD was to increase sensitivity in cases where the filling factor is low [26]. In porous materials, for instance, the size of the detector is determined by the geometry of the porous matrix (e.g. a sandstone rock), rather than the volume of the detectable spins. Decreasing the volume of the detector to increase sensitivity is only possible if the sensor can be transported and the signal can be concentrated. Flow provides such an opportunity since the fluid is naturally transported to a location outside of the bulky matrix. The sensor must be able to retain the encoded information during transport, which for RD is satisfied when the longitudinal relaxation time is longer than the timescale of the fluid flow from encoding to detection.

While the remote detector can be made considerably more sensitive than the encoding coil, it is still not obvious that a sensitivity gain is achieved in the RD scheme. First and foremost, the addition of an extra experimental dimension means considerably longer acquisition times. Noise due to the addition of this extra dimension may then be susceptible to multiplicative or t_1 noise which can degrade the remote spectrum or image [27], similar to the effect of noise on the indirect dimension of a two-dimensional NMR spectrum. Finally, relaxation during transport can cause significant loss in signal by the time the spins are detected.

Granwehr and Seeley analyzed the sensitivity of RD in detail for transient signals such as an FID and for point-by-point experiments such as pure phase encoding for imaging [28]. For

Please cite this article in press as: E. Harel, Lab-on-a-chip detection by magnetic resonance methods, Prog. Nucl. Magn. Reson. Spectrosc. (2010), doi:10.1016/j.pnmrs.2010.05.002

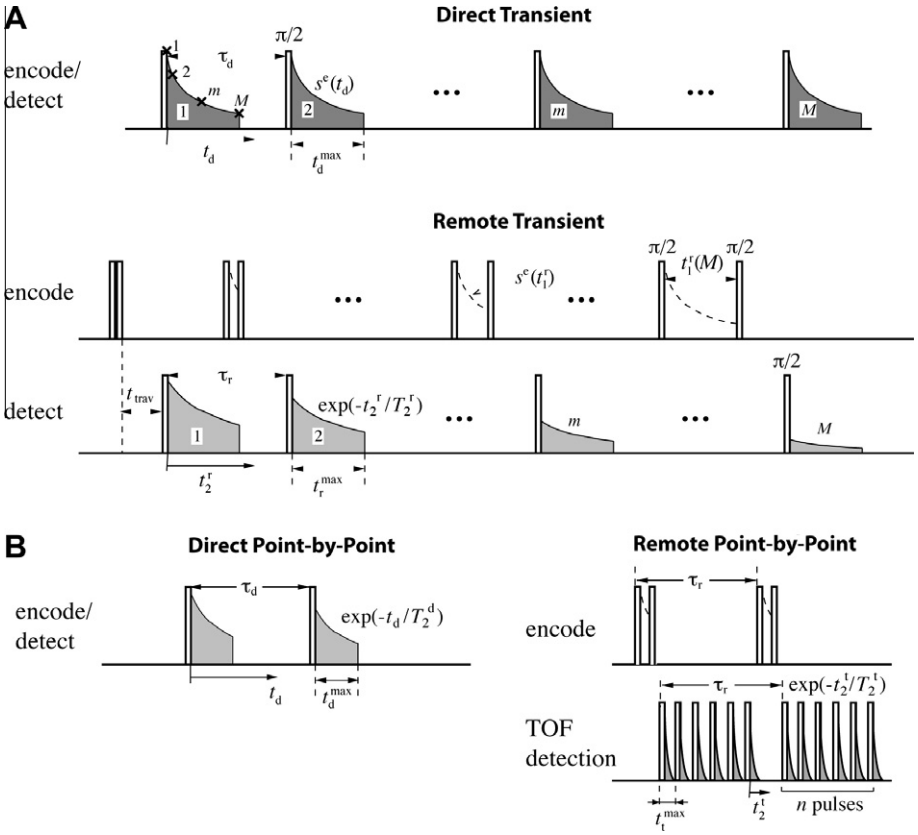

Fig. 5. Remote versus direct detection. (A) Comparison of an FID detected transiently and one constructed from an interferogram assembled by incrementing the delay between an excitation and storage pulse. The directly detected signal as a function of t_d is dependent of the acquisition time per transient, t_d^{max}, number of scans, M, and recycle delay, τ_d. For remote detection, the signal is dependent on the travel time, t_{trav}, residence time, t_2^{max}, number of indirect time points, M, and relaxation times in the encoding and detection region. $2M$ encoding steps are needed to reconstruct the FID in the remote detection scheme, corresponding to an equivalent number of signal averaging steps in direct detection to obtain the same total acquisition time minus the overhead due to the travel time of the flowing spins. (B) Comparison of point-by-point detection such as pure phase encoding of remote and direct detection. In direct detection, each k-space point is given by the integrated signal after an excitation pulse. The decay of the signal is given by T_2^d, which may be shortened by field inhomogeneities caused by susceptibility gradients. In remote detection, the signal is read out in the detector where it is subject to T_2^r, which because of the more favorable field environment is typically longer than T_2^d. When applying TOF detection, the additional sensitivity enhancement may be sacrificed for increased temporal resolution during flow by prematurely cutting off the FID versus single-step detection.

spectroscopy, they compared a remotely detected spectrum to a direct, two-dimensional NMR experiment. Fig. 5A illustrates the relative parameters needed to describe a transient signal recorded by a direct and the equivalent remote detection experiment. In direct detection, the SNR, Ψ_d, from a single point along the transient at a time t_d is related to the signal envelope, $s^e(t)$, total evolution time, t_d^{max}, and repetition time, τ_d, according to

$$\Psi_d = \frac{s^e(t_d)}{\rho_d}\sqrt{\frac{t_d^{max}}{\tau_d}}, \tag{13}$$

where ρ_d is the square root of the power spectral density. If a given number of points, M, are recorded during the transient time in the direct dimension, then the same number of separate indirect points must be recorded in the remote experiment. To accurately record the complex signal in RD, which is typically done in quadrature detection, two encoding steps are necessary to recover the lost phase of the signal. Because sensitivity is defined as the SNR per square root of time, it is necessary to signal average the directly detected spectrum for the duration of the total acquisition time in the remote detection scheme for a fair comparison. This roughly corresponds to $2M$ signal-averaging steps of the directly detected transient signal.

For a remotely detected experiment, the sensitivity, Ψ_r, for each complex data point is given by

$$\Psi_r = \frac{s^e(t_1^r)}{\rho_r}\sqrt{\frac{T_2^r}{4\tau_r}\left(1-\exp\left(-\frac{2t_r^{max}}{T_2^r}\right)\right)}, \tag{14}$$

where t_1^r is the evolution time in the encoding dimension, T_2^r and t_r^{max} are the relaxation and total evolution time in the remote detection dimension, respectively, and τ_r is the repetition time of the pulse train from the remote coil. The above equation neglects the finite travel time of the spins and longitudinal relaxation during transport. From Eqs. (13) and (14), the relative sensitivity, Ψ_r/Ψ_d, between remote and direct detection can be found. Two cases are of interest for LOC applications. The first is appropriate in continuous flow mode in which the FID prematurely decays due to the short residence time of the fluid inside the detection coil. The effective transverse time is shortened compared to stationary spins. In the other limiting case, the flow is stopped during detection so as to give the maximum signal in the remote coil. The relative sensitivity in these two cases is given by

$$\left[\frac{\Psi_r}{\Psi_d}\right]_{tran} \approx \frac{\Lambda}{\sqrt{2}}\sqrt{\frac{T_2^r}{2t_d^{max}}}, \quad t_r^{max} > T_2^r; \tag{15}$$

$$\left[\frac{\Psi_r}{\Psi_d}\right]_{tran} \approx \frac{\Lambda}{\sqrt{2}}, \quad t_r^{max} \ll T_2^r; \tag{16}$$

where $\Lambda = s^e(t_1^r)/s^e(t_d)$ is the relative sensitivity of the remote and direct detectors for the same sample under identical experimental conditions. The factor of $\sqrt{2}$ is a consequence of the need to perform two separate experiments for reconstructing the complex FID in RD, equivalent to quadrature detection in the direct case. It is important to realize that the relative sensitivity is independent of the number of points recorded in the FID.

Please cite this article in press as: E. Harel, Lab-on-a-chip detection by magnetic resonance methods, Prog. Nucl. Magn. Reson. Spectrosc. (2010), doi:10.1016/j.pnmrs.2010.05.002

The theoretical gain in sensitivity of RD given by Eq. (16) can only be realized in ideal conditions. In practice, the longitudinal relaxation of the spins during transport and hydrodynamic dispersion can cause significant loss in sensitivity. If the fluid is significantly dispersed during transport than it is effectively diluted during detection, meaning that several detection pulses may be needed to detect all the encoded spins, adding noise to the spectrum and adversely affecting the sensitivity. However, if the signal is below the LOD in the direct experiment, RD may be the only way to obtain a spectrum in the first place.

For a point-by-point experiment (Fig. 5B), the situation is significantly more favorable for RD. At very high spatial resolutions, pure phase encoding is often the only way to reduce the blurring effects of diffusion [29]. Because phase encoding, also known as constant-time encoding, is a point-by-point method, it is comparable to RD since the same number of encoding steps are needed as with direct detection. The relative sensitivity is then given by

$$\left[\frac{\Psi_r}{\Psi_d}\right]_{pp} \approx \frac{\Lambda}{\sqrt{2}}\sqrt{\frac{T_2^r}{T_2^d}}. \tag{17}$$

An additional gain in sensitivity is achieved over direct detection if the transverse relaxation time during encoding, T_2^d, is significantly shorter than that of the detection environment, T_2^r. This criteria is evident in LOC devices where susceptibility gradients due to the geometry of the chip can cause severe line broadening, several orders of magnitude larger than the linewidths in the detector.

4.5. Dispersion measurements using time-of-flight

As discussed earlier, magnetic resonance imaging is capable of measuring the local velocity distribution of fluid displacements. Spins are ideal tracers of flow because manipulating them does not affect the liquid's hydrodynamic properties. Since RD records the TOF of encoded spins to the detector, it is capable of obtaining a macroscopic scale view in the long-time regime of flow [30]. Local velocities are averaged away, but the long time-scale dynamics are preserved – a feature that makes remote detection complementary to motion encoding measurements with pulsed gradient methods.

To get adequate temporal resolution in the TOF curves, the detection coil volume, V_d, is made smaller than the encoded fluid volume. A train of detection pulses separated by the average residence time of encoded spins in the detection coil, records an FID whose integrated intensity corresponds to exactly one point along the indirect domain of the imaging or spectroscopic experiment. For imaging, a series of snapshots is formed showing the spatial distribution of spins with a specific TOF value. If the detection pulses are properly spaced in time such that no encoded spins go undetected, the sum of all the partial images is equivalent to a direct image, weighted by an exponential damping of the TOF for each pixel by the longitudinal relaxation time, T_1. Therefore, spin magnetization that never reaches the detector either because of stagnation or because of complete relaxation is not detected and shows up as voids in the remote images. If hydrodynamic dispersion is present, then the signal is appropriately scaled as each partial images is spatially dispersed as shown in Fig. 6 [28]. In the TOF dimension, this is manifested as a broadening of the TOF curve.

The remote detection signal as a function of position and TOF is given by

$$S(\mathbf{r}, t_{TOF}) = e^{-t_{TOF}/T_1}\frac{S_0}{V_d}\int_{\det.} d\mathbf{r}_d \int_{voxel} d\mathbf{r}'\,\rho(\mathbf{r}')P_s(\mathbf{r}_d, t_{TOF}), \tag{18}$$

where S_0 is the signal per unit volume of encoded spins, T_1 is the longitudinal relaxation time, $\mathbf{r}$ is the position of an encoded voxel, $\mathbf{r}'$ is the position of a volume element in the detector, and ρ is the spin density. P_s is the flow propagator that gives the conditional probability of a fluid at position $\mathbf{r}'$ at time zero to be found in the detector a time t_{TOF} later. The TOF curves provide the mean and variance of $S(\mathbf{r}, t_{TOF})$. If one replaces the propagator with an averaged propagator, then the mean and variance of the signal $S(\mathbf{r}, t_{TOF}) = NS_0 e^{-t_{TOF}/T_1}\overline{P}(\mathbf{r}, t_{TOF})$, are proportional to the average flow velocity and hydrodynamic dispersion of the encoded fluid. If the detector is spatially resolved then the propagator is only averaged over the encoded voxel and approaches the true propagator in the Eulerian view of flow [31]. Unlike pulse-gradient spin echo (PGSE) methods [10] that determine the local fluid displacements of a voxel centered at $\mathbf{r}$, which is the Lagrangian view of flow, the RD propagator is a measure of the average velocity and dispersion over global displacements (i.e. much greater than the voxel dimension).

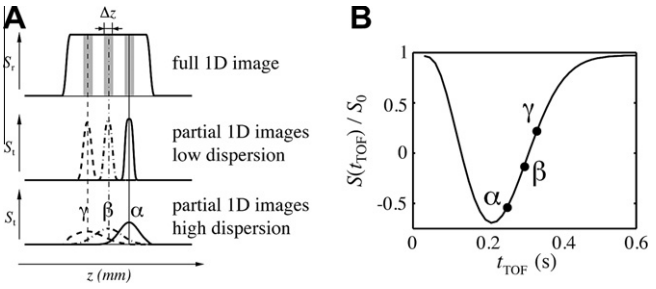

Fig. 6. (A) Effects of dispersion on the image reconstruction of a flowing sample. The full image can be faithfully reconstructed by summing together the partial images obtained from each point, α, β, and γ in the TOF curve. This image is weighted by the longitudinal relaxation time of the sensor during travel. When the dispersion is low relative to the spatial resolution, each partial image corresponding to a particular TOF value has the same amplitude as the corresponding slice in the full image. For high dispersion, the amplitude is lowered and the signal becomes spread across multiple TOF values. (B) Travel curve showing the location of partial images in (A) at different TOF values.

5. Remote detection of lab-on-a-chip

5.1. Hardware

RD requires specialized hardware for its implementation. An auxiliary probe [32] houses the detector and RF circuit (Fig. 7), which is isolated from the encoding probe. The RF tank circuit is soldered to a circuit board and mounted onto a Teflon support that is housed inside a modular probe body. The probe assembly can be positioned from either below or above the magnet bore allowing for flexibility in integrating with an additional commercial RF probe. The fluid flows from the encoding coil, typically an RF small-animal imaging probe, to the detection coil which is a 500-μm ID solenoid wrapped tightly around a sleeve that surrounds 360 μm OD, 150 μm ID PEEK capillary tubing. The detection coil is immersed in FC-43 susceptibility matching fluid to achieve improved field homogeneity [33]. The LOC device is positioned inside a custom-built Teflon holder that accepts the various fluidic connections. The holder is compact enough to fit tightly inside the encoding coil. A brass or copper shield is placed over the detection coil and circuit to isolate it from the encoding coil during RF irradiation.

Since two probes are used for excitation and detection, two separate channels on the spectrometer are needed. For xenon experiments, it is possible to use two lowband amplifiers, one for transmit/receive (detection) step of the experiment and the other for transmit only (encoding). However, for proton (highband) experiments, an external amplifier is needed for the encoding part of the experiment. An external amplifier is connected to one of the decoupler channels, which allows for the pulse shaping capabilities needed in some of the pulse sequences. The external and internal amplifiers have different gains so it is necessary to calibrate each

Please cite this article in press as: E. Harel, Lab-on-a-chip detection by magnetic resonance methods, Prog. Nucl. Magn. Reson. Spectrosc. (2010), doi:10.1016/j.pnmrs.2010.05.002

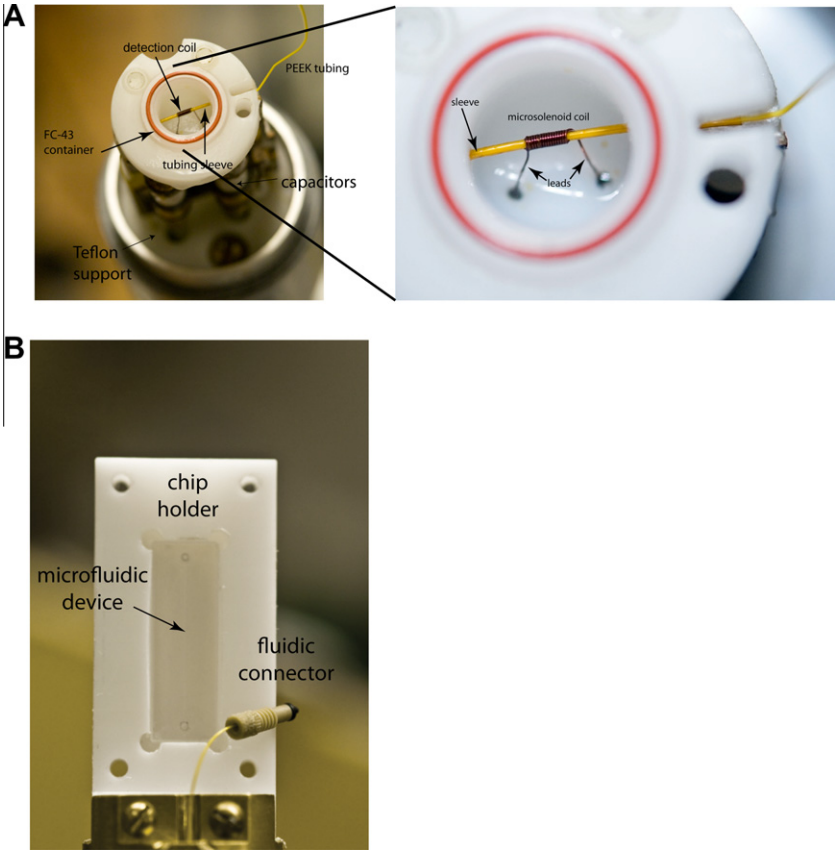

Fig. 7. Remote detection hardware. (A) Top view of remote detection probe housing containing RF circuit and microsolenoid coil. The fluid flows from the encoding region where the chip is held (B) through PEEK capillary tubing (Upchurch Scientific) to the microsolenoid detector, which is immersed in FC-43 (3M Corporation) susceptibility matching fluid for improved homogeneity. The capillary and RF coil are easily interchangeable depending on the specific experiment. The connections to the LOC device are made without any need for adhesives or glue using rubber ferrules and threaded connectors to make the seal. The Teflon chip holder fits snuggly inside a commercial 30 mm RF imaging probe (Varian Inc.).

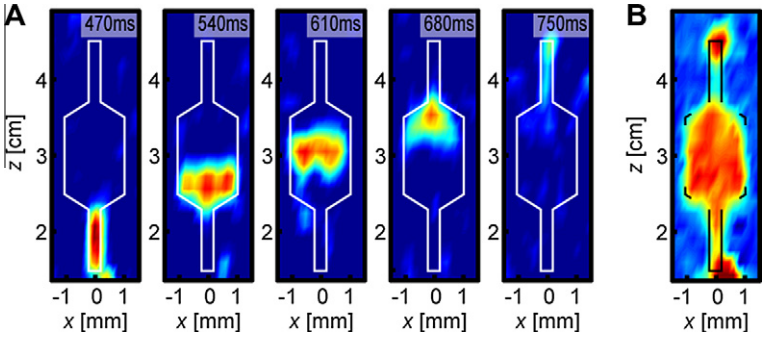

Fig. 8. Two-dimensional image of Xe^{129} gas flow parallel to the face of an LOC device, along the *x* and *z*-axes. (A) Partial images of gas originating in the channel of the chip (outlined in white), shown for gas flowing from top to bottom, for different TOF values between the encoding location and detection coil. (B) Full image of the perfused areas in the chip, reconstructed by summing the data shown in (A) over all TOF values. Reprinted with permission from Hilty et al. [38].

separately, for example, when setting the 90° pulse duration for the various pulse sequences. The external amplifier is triggered by the spectrometer for proper gating, so that unwanted power is not passed to the encoding probe during detection. The gating is supplied by a TTL trigger from one of the external outputs of the spectrometer, which is controlled by specific commands in the pulse sequence.

5.2. Xenon-129 imaging

Prior to the use of RD of fluids inside LOC devices, the technique was primarily used for examining flow of Xe^{129} gas in porous materials such as rocks [34] and silica aerogel [35]. Xe^{129}, which is spin-1/2, is remarkable as a tracer because it exhibits an extreme sensitivity to its chemical environment, exhibiting a range of more than 7000 ppm in chemical shift. Equally remarkable is its ability to become hyperpolarized through spin-exchange with optically pumped rubidium atoms [36]. In this state, xenon is four orders of magnitude more polarized than at thermal equilibrium. In addition, xenon has a longitudinal relaxation time of several minutes making it an ideal tracer for remote detection experiments. Finally, gas flow is extremely stable and reproducible over many hours, making it suitable for point-by-point Fourier experiments where phase stability is crucial.

Please cite this article in press as: E. Harel, Lab-on-a-chip detection by magnetic resonance methods, Prog. Nucl. Magn. Reson. Spectrosc. (2010), doi:10.1016/j.pnmrs.2010.05.002

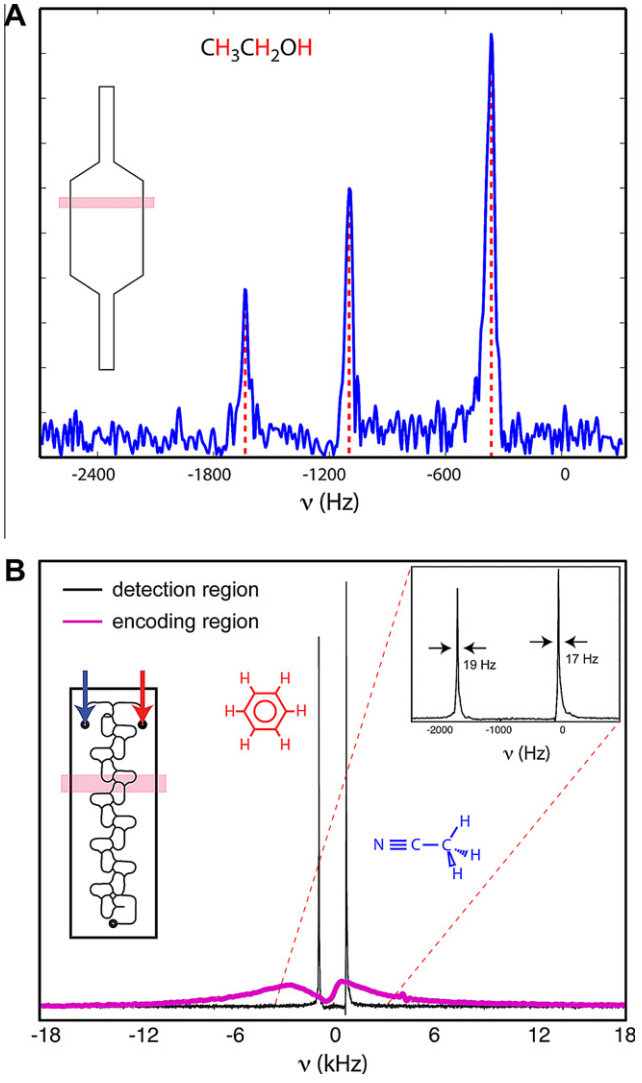

Fig. 9. (A) Remotely reconstructed ^{1}H spectrum at 300 MHz of ethanol in a 0.5-mm slice through a single-channel LOC device. The spectrum is acquired by Fourier transformation of an indirect interferogram formed by incrementing the delay between excitation and storage pulses so as to sample the complex phase evolution of the FID. A spectrum is acquired for each detection pulse. (B) Direct spectrum (magenta) of stationary fluid composed of a mixture of benzene and acetonitrile through a complex 3D LOC device. Inset: Spectrum of fluids inside the detection region after flowing out of the LOC device. (For interpretation of the references to color in this figure legend, the reader is referred to the web version of this paper.)

For gas flow applications, hyperpolarization coupled to RD allows MR to be performed on an LOC device [37]. Hilty et al. [38], flowed xenon gas through a simple, single channel device, demonstrating the ability to resolve, both spatially and temporally, the fluid flow. Shown in Fig. 8 are a series of panels that represent the spatially resolved origin of xenon spin density that arrive in the detector at given time after encoding. For unidirectional flow as in a single channel chip, earlier TOF images correspond to spins near the outlet of the chip, while later TOF images correspond to those near the inlet. The spatial distribution of spins provides information on dispersion and diffusional mixing. A flat profile indicates that the fluid has adequately sampled the image area during the timescale of the spatial encoding, while the degree of curvature is indicative of the degree of nonuniformity in the velocity field.

It is important to realize that these partial images of the spin density are fundamentally different from other flow measurements. One salient difference is that only spins that reach the detector before the longitudinal relaxation time of the fluid are detected. Fluid that is stagnant or has too low a velocity to reach the detector within T_1 is never imaged. While this is a limitation for slow moving fluids, it provides a tremendous advantage by eliminating any background due to the substrate or stationary spins. For proton imaging, this offers a method for very sensitive detection of small volumes of flowing fluid even in the presence of an otherwise massive background signal from the sample matrix.

5.3. Liquids

While utilizing xenon gas as a tracer functioned as an important first-step in realizing the potential of combining MRI and LOC, the vast majority of fluidic applications involve liquid flow. Furthermore, the power of NMR is in its ability to obtain chemical specificity through the chemical shift. Unfortunately, for applications in LOC, the field inhomogeneity caused by the deviations of cylindrical symmetry along the static field axis for most practical chip designs, is too great for resolving proton chemical shifts. This can be appreciated by considering the spectra on and off various LOC chip designs as shown in Fig. 9. For simple chip geometries such as the one used in the xenon imaging study, the spectral resolution of a few millimeter slice normal to the static field direction is relatively high. A remotely reconstructed ethanol spectrum clearly shows the three proton peaks. The sensitivity is too poor to obtain a direct spectrum with the RF imaging coil used for excitation. While planar probes could provide significantly higher sensitivity and resolution in this case, the ability to select any arbitrary region of the sample using imaging gradients is sacrificed. In Fig. 8B, the spectrum of a similar thickness slice of a more complex LOC device shows the severe field distortions caused by susceptibility mismatch at the material boundaries. The two components, benzene and acetonitrile are not resolved on the chip itself where the linewidth exceeds 5 kHz. In contrast, the spectrum off the chip and inside the detection coil as shown in the inset clearly shows the two well-resolved resonances.

Poor spectral resolution on the LOC device presents a formidable challenge to attempt to understand the dynamics of multiple-component fluid flow, as efficient spatial tagging of the different components is limited due to the fast flow rates and gradient encoding artifacts. In RD, however, spectral separation is a natural consequence of the detection modality because the various fluid components retain their chemical-shift signatures even after flowing out of the microfluidic device [39]. As shown in Fig. 10, water and ethanol can be distinguished in a single experiment by detecting their spectrum outside of the encoding region where the homogeneity is very poor. As long as the residence time of the fluid is longer than the inverse of the chemical-shift separation of the various species, each can be individually imaged as shown for this simple T-chip geometry, regardless of the inhomogeneity in the chip.

For a given flow rate, the residence time in the detector is proportional to the coil length if one assumes plug flow. Even in the case of Taylor dispersion, where the velocity across the tube has a parabolic profile, one can still relate the residence time to a mean flow rate and detection volume. If two species are close in chemical shift, one needs to adjust the coil length or alternatively adjust the flow rate so that the effective transverse relaxation time is sufficiently long for adequate spectral resolution. However, increasing the coil volume effectively decreases the time resolution of the experiment since each detection pulse must be separated, at least optimally, by the residence time. In essence, the time scale of observation of the FID limits the certainty of the chemical shift. Recently, it was shown that this limitation could be overcome by introducing another degree of freedom that couples directly to

Please cite this article in press as: E. Harel, Lab-on-a-chip detection by magnetic resonance methods, Prog. Nucl. Magn. Reson. Spectrosc. (2010), doi:10.1016/j.pnmrs.2010.05.002

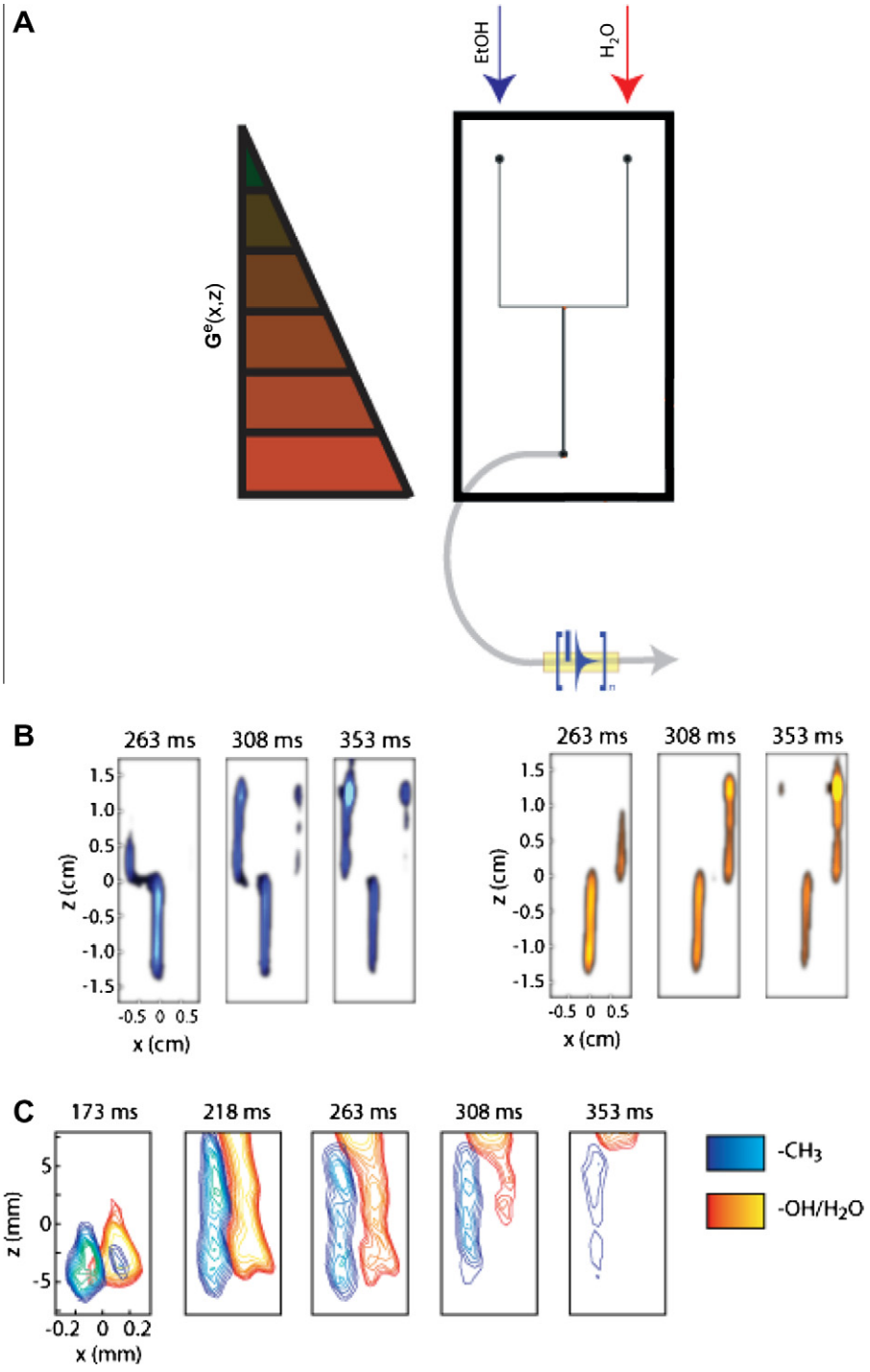

Fig. 10. Liquid flow imaging through a simple microfluidic chip. (A) Ethanol (*blue arrow*) and water (*red arrow*) flow through a T-mixer chip. The detection volume is less than 50 nL. (B) Spectra. Even though the spectra are not resolvable inside the chip, they are resolved outside of it. The flow of each species can be distinguished and subsequently imaged by selecting the appropriate resonance peak in the detector. (C) A zoomed-in view of the mixing region shows that the fluids do not effectively mix under these flow condition. (For interpretation of the references to color in this figure legend, the reader is referred to the web version of this paper.) Reprinted with permission from Harel et al. [39].

the temporal resolution of the observation, while being independent of the frequency evolution during the FID [40]. Imaging gradients can serve precisely this function. By spatially resolving the detection, one can artificially slice the detector into multiple, but smaller detectors, each with a short residence time and, hence, a high temporal resolution. At the same time, the FID occurs throughout the entire, long detector so T_2 is still long. Sub-millisecond time resolution can be achieved in this way as long as sufficient sensitivity exists to subdivide the detection volume.

To better understand the way in which the time resolution is increased by means of adding a gradient dimension in the encoding region, consider a small region of a fluidic device near the outlet as shown in Fig. 11A. Each voxel contains either one or both of the fluid components, which are encoded according to the scheme de-

Please cite this article in press as: E. Harel, Lab-on-a-chip detection by magnetic resonance methods, Prog. Nucl. Magn. Reson. Spectrosc. (2010), doi:10.1016/j.pnmrs.2010.05.002

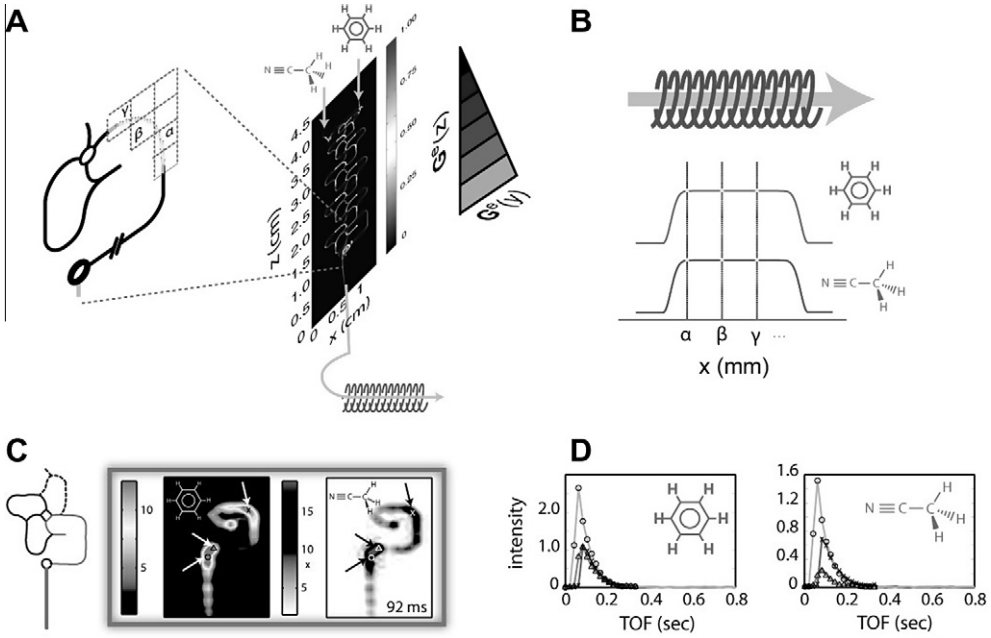

Fig. 11. (A) Left – Schematic of remote detection with time slicing of the TOF dimension at 300 MHz. A spectroscopic image (B) is formed in the detector with each position along the 1D profile corresponding to a different TOF value of encoded spins. Right – Direct image of face of LOC mixing device using spin echo pulse sequence (SEMS) on stationary flow. Acquisition time is nearly 10 h. (C) Partial images taken from the integrated data set near the outlet of the device. The temporal resolution is 2 ms obtained by imaging the remote detector with a 20-ms residence time with 10-pixel resolution. By obtaining a spectroscopic image in the detector, each species (acetonitrile and benzene) can be selected in the post-processing of the data to obtain different partial images of the flow. (D) For each point in the image a TOF curve is measured which gives information about the time of arrival and dispersion of the encoded fluid voxel. Differences at the outlet (marked with a triangle symbol) show that the fluid species begin to separate in the dead volume near the outlet connector. Reprinted with permission from Harel and Pines [40].

scribed above. The earlier encoded voxel to arrive (labeled α) is nearer to the outlet. If this voxel is smaller than the detection volume it represents a section of the 1D profile along the detection coil axis. Some dispersion occurs so that this voxel may be spread over a larger volume than initially encoded. The spatial resolution along the detection coil axis therefore determines to what degree the initial voxel can be resolved in time. Since the chemical species are assumed not to change while flowing through the LOC device, a spectrum of the mixture is recorded for each detection pulse as shown in Fig. 11B. By selecting a peak over which to integrate in the post-processing of the multidimensional data set, an image is reconstructed for each chemical species. The spectral resolution of this spectrum is determined by the residence time in the detection coil and the separation between detection pulses during stroboscopic acquisition.

The enhancement is demonstrated by recording chemically resolved fluid mixing of benzene and acetonitrile through a complex microfluidic device at an unprecedented temporal resolution corresponding to faster than 500 frames per second. The inadequacy of direct detection is best illustrated by considering the image of the chip shown in Fig. 11A. The 2D image is a result of 10 h signal averaging using a standard spin-echo imaging sequence (SEMS) of water under stationary conditions. During flow, no image is formed as the high velocity rapidly dephases the spins. While one could envision using velocity compensating pulse sequences, the fast flow, low sensitivity, and extreme demands of gradient switching at such high gradient fields necessary for the high spatial resolution, makes direct imaging of limited utility.

6. Conclusion

While RD provides a rich body of information with high sensitivity, it suffers from its inherently slow point-by-point acquisition. Most limiting is the fact that the encoded fluid packet must reach the detector within the sometimes-short T_1 relaxation time of the spins. Therefore, coupling direct detection with remote detection may prove beneficial in several ways. For one, the ability to record an image both directly and remotely can give insight into stagnant fluid and recalculating or turbulent flow since these will give rise to a signal in the former, but not in the latter. Of course, this assumes that the signal is sufficiently strong to see a direct image in the first place.

Another possibility could be to place microcoils near the inlet of the LOC device, for example, by wrapping microsolenoid coils around the capillary tubing, to label spins more efficiently than achievable with volume-selective RF pulses. Spins from each input channel could be labeled by inversion in separate experiments and then followed by imaging and spectroscopy on and off the chip. Correlating the spectrum prior to and after mixing may provide new insight into chemical reactions [41]. By following the dynamics inside the LOC mixing device itself, detection of previously inaccessible intermediate states at a high temporal resolution may also become feasible.

Advances in microfabrication methods will undoubtedly bring LOC to more mainstream use in the MR community. Highly sensitive microsolenoid coils have already helped bring MR and liquid chromatography (LC) together [42]. With the introduction of LOC platforms, LC may be performed directly on the device, instead of coupling to external columns. More sophisticated fabrication methods are constantly lowering the achievable LOD. Three-dimensional coil geometries are being pursued to bring the sensitivity of solenoid microcoils to planar structures [43]. While these coils are currently less sensitive than hand-wound microcoils and even planar coil structures, they may prove promising in the future when issues of susceptibility mismatch and spectral resolution are properly addressed.

The field of NMR on a chip is still relatively young and efforts along both fronts will be sure to advance MR towards the stature that optical methods currently enjoy. The powerful analytical and

Please cite this article in press as: E. Harel, Lab-on-a-chip detection by magnetic resonance methods, Prog. Nucl. Magn. Reson. Spectrosc. (2010), doi:10.1016/j.pnmrs.2010.05.002

noninvasive nature of MR make it ideally suited for LOC, and with the advent of commercial hyperpolarization methods such as dynamic nuclear polarization (DNP) [44], even smaller sample volumes and concentrations will be within reach.

Acknowledgments

Discussions, encouragement, and support from Professor Alex Pines is greatly appreciated.

References

[1] H.A. Stone, A.D. Stroock, A. Ajdari, Annu. Rev. Fluid Mech. 36 (2004) 381.
[2] S.J. Haswell, R.J. Middleton, B. O'Sullivan, V. Skelton, P. Watts, P. Styring, Chem. Commun. 5 (2001) 391.
[3] M.U. Koop, A.J. de Mello, A. Manz, Science 280 (1998) 1046.
[4] D. Figeys, D. Pinto, Electrophoresis 22 (2001) 208.
[5] Y. Liu, C.D. Garcia, C.S. Henry, Analyst 128 (2003) 1002.
[6] S. Devasebathipathy, J.G. Santiago, S.T. Wereley, C.D. Meinhart, K. Takehara, Exp. Fluids 34 (2001) 504.
[7] D. Ross, L.E. Locascio, Anal. Chem. 75 (2003) 1218.
[8] L. Zhu, C.S. Lee, D.L. DeVoe, Lab Chip 6 (2006) 115.
[9] S.-A. Leung, R.F. Winkle, R.C.R. Wootton, A.J. de Mello, Analyst 5 (2005) 431.
[10] P.T. Callaghan, Principles of Nuclear Magnetic Resonance Microscopy, Oxford University Press, Oxford, 1991.
[11] E. Breitmaier, Structure Elucidation by NMR in Organic Chemistry, Wiley, New York, 1993.
[12] K. Wüthrich, NMR of Proteins and Nucleic Acids, Wiley, New York, 1986.
[13] D.I. Hoult, R.E. Richards, J. Magn. Reson. 24 (1976) 71.
[14] T.L. Peck, R.L. Magin, P.C. Lauterbur, J. Magn. Reson. 108 (1995) 114.
[15] A.G. Webb, Prog. Nucl. Magn. Reson. Spectrosc. 31 (1997) 1.
[16] C. Massin, F. Vincent, A. Homsy, K. Ehrmann, G. Boero, P.-A. Besse, A. Daridon, E. Verpoorte, N.F. de Rooij, R.S. Popovic, J. Magn. Reson. 164 (2003) 242.
[17] H. Wensink, F. Benito-Lopez, D.C. Hermes, W. Verboom, H.J.G.E. Gardeniers, D.N. Reinhoudt, A. van den Berg, Lab Chip 5 (2005) 280.
[18] A. Homsy, J. Lichtenberg, C. Massin, F. Vincent, P.-A. Besse, R.S. Popovic, N.F. de Rooij, E. Verpoorte, in: Proceedings of Micro Total Analysis Systems, Nara, Japan, 3–7 November 2002, Kluwer Academic Publishers, Dordrecht, 2002, p. 115.
[19] J. Bart, J.W.G. Janssen, P.J.M. van Bentum, A.P.M. Kentgens, J.G.E. Gardeniers, J. Magn. Reson. 201 (2009) 175.
[20] Y. Maguire, I.L. Chuang, S. Zhang, N. Gershenfeld, Proc. Natl. Acad. Sci. USA 104 (2007) 9198.
[21] K. Ehrmann, M. Gersbach, P. Pascoal, F. Vincent, C. Massin, D. Stamou, P.-A. Besse, H. Vogul, R.S. Popovic, J. Magn. Reson. 178 (2006) 96.
[22] S. Ahola, F. Casanova, J. Perlo, K. Munnemann, B. Blumich, S. Stapf, Lab Chip 6 (2006) 90.
[23] B.S. Akpa, S.M. Matthews, A.J. Sederman, K. Yunus, A.C. Fisher, M.L. Johns, L.F. Gladden, Anal. Chem. 79 (2007) 6128.
[24] A.J. Moule, M.M. Spence, S.I. Han, J.A. Seeley, K.L. Pierce, S. Saxena, A. Pines, Proc. Natl. Acad. Sci. USA 100 (2003) 9122.
[25] S. Xu, V.V. Yashchuk, M.H. Donaldson, S.M. Rochester, D. Budker, A. Pines, Proc. Natl. Acad. Sci. USA 103 (2006) 12668.
[26] J.A. Seeley, S.-I. Han, A. Pines, J. Magn. Reson. 167 (2004) 282.
[27] J. Granwehr, Appl. Magn. Reson. 32 (2007) 113.
[28] J. Granwehr, J.A. Seeley, J. Magn. Reson. 179 (2006) 280.
[29] M. Weiger, D. Schmidig, S. Denoth, C. Massin, F. Vincent, M. Schenkel, M. Fey, Concepts Magn. Reson. B 33B (2008) 84.
[30] J. Granwehr, E. Harel, C. Hilty, S. Garcia, L. Chavex, A. Pines, P.N. Sen, Y.-Q. Song, Magn. Reson. Imaging 25 (2007) 449.
[31] J.D. Seymour, P.T. Callaghan, AIChE J. 43 (1997) 2096.
[32] S. Han, J. Granwehr, S. Garcia, E.E. McDonnell, A. Pines, J. Magn. Reson. 182 (2006) 260.
[33] D.L. Olson, T.L. Peck, A.G. Webb, R.L. Magin, J.V. Sweedler, Science 270 (1995) 5244.
[34] J. Granwehr, E. Harel, S.-I. Han, S. Garcia, P.N. Sen, Y.-Q. Song, A. Pines, Phys. Rev. Lett. 95 (2005) 075503.
[35] E. Harel, J. Granwehr, J. Seeley, A. Pines, Nat. Mater. 5 (2006) 321.
[36] B.M. Goodson, J. Magn. Reson. 155 (2002) 157.
[37] E.E. McDonnell, S.-I. Han, C. Hilty, K. Pierce, A. Pines, Anal. Chem. 77 (2005) 8109.
[38] C. Hilty, E.E. McDonnell, J. Granwehr, K.L. Pierce, S.-I. Han, A. Pines, Proc. Natl. Acad. Sci. USA 102 (2005) 14960.
[39] E. Harel, C. Hilty, K. Koen, E. McDonnell, A. Pines, Phys. Rev. Lett. 98 (2007) 017601.
[40] E. Harel, A. Pines, J. Magn. Reson. 193 (2008) 199.
[41] M. Sabieh, C. Hilty, C. Chu, L.S. Bouchard, K. Pierce, A. Pines, Anal. Chem. 79 (2007) 2806.
[42] N. Wu, T.L. Peck, A.G. Webb, R.L. Magin, J.V. Sweedler, Anal. Chem. 66 (1994) 3849.
[43] M.H.C. Lam, M.A. Homenuke, C.A. Michal, C.L. Hansen, J. Micromech. Microeng. 19 (2009) 095001.
[44] W.A. Baker, Rev. Mod. Phys. 34 (1962) 173.

Glossary

COSY: correlation spectroscopy
DNP: dynamic nuclear polarization
FEM: finite-element modeling
FID: free-induction decay
LC: liquid chromatography
LIF: laser-induced fluorescence
LOC: lab-on-a-chip
LOD: limit-of-detection
MR: magnetic resonance
MRI: magnetic resonance imaging
PGSE: pulsed gradient spin echo
RD: remote detection
SEMS: spin echo multislice
SNR: signal-to-noise
TEM: transverse electromagnetic mode
TOF: time-of-flight

Please cite this article in press as: E. Harel, Lab-on-a-chip detection by magnetic resonance methods, Prog. Nucl. Magn. Reson. Spectrosc. (2010), doi:10.1016/j.pnmrs.2010.05.002